RESEARCH ARTICLE

CARBON ENERGY WILEY

Electrodeposition of a dendrite-free 3D Al anode for improving cycling of an aluminum–graphite battery

Junfeng Li[1] | **Kwan San Hui[2]** | **Shunping Ji[1]** | **Chenyang Zha[1]** | **Chengzong Yuan[1]** | **Shuxing Wu[3]** | **Feng Bin[4]** | **Xi Fan[5]** | **Fuming Chen[6]** | **Zongping Shao[7,8]** | **Kwun Nam Hui[1]**

[1]Joint Key Laboratory of the Ministry of Education, Institute of Applied Physics and Materials Engineering, University of Macau, Avenida da Universidade, Taipa, China

[2]School of Engineering, Faculty of Science, University of East Anglia, Norwich, UK

[3]School of Chemical Engineering and Light Industry, Guangdong University of Technology, Guangzhou, China

[4]State Key Laboratory of High-Temperature Gas Dynamics, Institute of Mechanics, Chinese Academy of Sciences, Beijing, China

[5]Ningbo Institute of Materials Technology, Engineering, Chinese Academy of Sciences, Ningbo, China

[6]Guangdong Provincial Key Laboratory of Quantum Engineering and Quantum Materials, School of Physics and Telecommunication Engineering, South China Normal University, Guangzhou, China

[7]State Key Laboratory of Materials-Oriented Chemical Engineering, College of Chemical Engineering, Nanjing Tech University, Nanjing, China

[8]WA School of Mines: Minerals, Energy and Chemical Engineering (WASM-MECE), Curtin University, Perth, Australia

Correspondence
Kwan San Hui, School of Engineering, Faculty of Science, University of East Anglia, Norwich NR4 7TJ, UK.
Email: k.hui@uea.ac.uk

Zongping Shao, State Key Laboratory of Materials-Oriented Chemical Engineering, College of Chemical Engineering, Nanjing Tech University, 211816 Nanjing, China.
Email: shaozp@njtech.edu.cn

Kwun Nam Hui, Joint Key Laboratory of the Ministry of Education, Institute of Applied Physics and Materials Engineering, University of Macau, Avenida da Universidade, 999078 Taipa, China.
Email: bizhui@um.edu.mo

Funding information
National Key Research and Development Program of China, Grant/Award Number: 2019YFE0198000; UEA funding; University of Macau,

Abstract

Aluminum–metal batteries show great potential as next-generation energy storage due to their abundant resources and intrinsic safety. However, the crucial limitations of metallic Al anodes, such as dendrite and corrosion problems in conventional aluminum–metal batteries, remain challenging and elusive. Here, we report a novel electrodeposition strategy to prepare an optimized 3D Al anode on carbon cloth with an uniform deposition morphology, low local current density, and mitigatory volume change. The symmetrical cells with the 3D Al anode show superior stable cycling (>450 h) and low-voltage hysteresis (~170 mV) at 0.5 mA cm^{-2}. High reversibility (~99.7%) is achieved for the Al plating/stripping. The graphite||Al-4/CC full batteries show a long lifespan of 800 cycles with 54 mAh g^{-1} capacity at a high current density of 1000 mA g^{-1}, benefiting from the high capacitive-controlled distribution. This study proposes a novel strategy to design 3D Al anodes for metallic-Al-based batteries by eliminating the problems of planar Al anodes and realizing the potential applications of aluminum–graphite batteries.

1 | INTRODUCTION

Aluminum–metal secondary batteries show remarkable potential as next-generation energy storage systems owing to their high theoretical gravimetric capacity (2.98 Ah g^{-1}), intrinsic safety, and abundant resource.[1–4] The development of high-energy cathode materials and low-cost and stable electrolytes has been extensively studied for aluminum-ion batteries and aluminum dual-ion batteries (consisting of a carbonaceous cathode).[5–12] However, as a crucial part of aluminum-based batteries, Al anodes have some challenging issues that need to be properly addressed, such as the dendrite growth, insulative oxide film, and corrosion accompanying hydrogen evolution in an ionic liquid (IL) electrolyte.[13–16]

Conventional Al anodes have the limitation of dendrite formation due to unstable reversible deposition, leading to safety concerns when piercing the separator and causing deteriorative capacity and cycling life.[14,17–19] In conventional aluminum–metal batteries with IL electrolytes, the ionic and electron passivating oxide layer hinders the connection between the electrolytes and the Al anodes and decreases the electrochemical activity of Al plating/stripping.[19,20] The passivating oxide layer tends to be consumed at the early electroredox process in batteries, exposing more Al anode to the corrosive electrolyte and increasing the side reaction and hydrogen evolution, especially in the presence of H$^+$ due to the air and moisture sensitivity of the IL electrolyte.[1,15] Therefore, the direct use of Al metal as anodes still poses a crucial challenge to the stability of aluminum–metal secondary batteries. Several strategies have been proposed to optimize the metallic Al anodes and to address these problems. Alloying of the Al metal with other elements, such as Al–Zn, Al–Cu, and Al–Ga, has been demonstrated to effectively alleviate the passivating oxide layer, resulting in a lower-energy-barrier interface and accomplishing the excellent Al plating/stripping electrochemical properties.[21–24] The treated Al anode by soaking or electroetching has shown particular interfacial chemistry with improved performance.[14,19,20] Although these studies have optimized the Al metal anodes, altering the planar nature of the Al anodes, which are vulnerable to dendritic and inhomogeneous deposition, is difficult.

Here, we successfully construct a 3D Al anode through electrodeposition on a 3D carbon cloth. Due to the advantages of the high special surface area and conductivity of the 3D structure, the obtained 3D Al anode (Al-4/CC) shows homogeneous Al deposition and a lower overpotential, eliminating the dendrite growth and promoting the reversibility of Al plating/stripping with the treated IL electrolyte. The symmetric cell fabricated using the optimized 3D Al anode delivers a long cycling time of 450 h with a low-voltage hysteresis of 170 mV, and a high Coulombic efficiency (CE) of approximately 99.7% is obtained for the Al reversible deposition. The 3D Al anode is assembled with a graphite cathode as the full battery, demonstrating an exceptional performance of approximately 54 mAh g^{-1} after 800 cycles at a high current density of 1000 mA g^{-1} with improved rate capability. This condition is attributed to the high capacitive-controlled contribution of the 3D Al anode.

2 | EXPERIMENTAL SECTION

2.1 | Materials

Natural graphite (mesh: 750–800, 99.95%), aluminum chloride (AlCl$_3$, AR, 99%), 1-ethyl-3-methylimidazolium chloride ([EMIm]Cl, 98.0%), and N-methyl-2-pyrrolidinone (NMP; AR) were provided by Aladdin. Aluminum pellets (Al, 1/4″ diameter × 1/4″ long, 99.999%) were purchased from Kurt J. Lesker Company. Carbon cloth (W0S1009) was purchased from Tanneng Co., Ltd., Taiwan, China.

2.2 | Preparation of the IL electrolyte

The IL electrolyte is prepared by sluggishly mixing AlCl$_3$ and [EMIm]Cl with a molar ratio of 1.3 in an argon-atmosphere glovebox ([O$_2$] <0.1 ppm, [H$_2$O] <0.1 ppm).

The mixing process must be slow, and continuous stirring is required to avoid a violent exothermal reaction; then, a light-yellow and transparent IL is obtained, which is called the original ionic liquid (IL-O) electrolyte. The treated ionic liquid (IL-T) electrolyte is obtained by treatment of the IL-O electrolyte with one high-purity Al pellet at 60°C for 24 h until it is nearly colorless.

2.3 | Materials' preparation and battery tests

2.3.1 | Preparation of electro-deposited Al on a carbon cloth (Al-X/CC) electrode

The carbon cloth (CC) current collectors are assembled against bare Al to prepare the deposited 3D Al electrode using the IL-O or IL-T electrolyte. The batteries discharge at $0.5\,\mathrm{mA\,cm^{-2}}$ with different discharge times to obtain different areal capacity depositions of Al on CC as a 3D Al anode.

2.3.2 | Preparation of the symmetric cells and Mo‖Al cells

For the symmetric cells, the Al-X/CC or bare Al as one electrode is assembled against another bare Al with an IL-O or IL-T electrolyte. Then, the symmetric cells are cycled at current densities of 0.25, 0.5, and $1\,\mathrm{mA\,cm^{-2}}$ for rate performance and at $0.5\,\mathrm{mA\,cm^{-2}}$ for plating and stripping performances. To test the CE, Al is plated on a Mo substrate at $0.5\,\mathrm{mA\,cm^{-2}}$ with $1\,\mathrm{mAh\,cm^{-2}}$ and stripped away by charging with a cut-off voltage of 0.5 V in the Mo‖Al cells.

2.3.3 | Preparation of the graphite/Al full batteries

In a typical process, the cathode is prepared by mixing a slurry with 80% graphite, 10% acetylene black, and 10% polyvinylidene difluoride in an NMP solvent. After that, the slurry is coated on a Mo current collector and dried at 80°C for 12 h in a vacuum. Ultimately, the areal loading of active materials is about $1.5\,\mathrm{mg\,cm^{-2}}$. The batteries are assembled with a graphite cathode and Al-X/CC or a bare Al anode. The full batteries are tested at a voltage window between 0.3 and 2.35 V for long cycling and rate performance at different rates of 100, 200, 500, and $1000\,\mathrm{mA\,g^{-1}}$.

All the Al-X/CC electrodes and batteries are prepared in soft-package cells with ~500 μL of electrolyte injected for each and tested by a multichannel battery tester (Neware BTS-53).

2.4 | Electrochemical measurements

The corrosion test is conducted in a three-electrode tank with Al-X/CC, CC, or an Al foil (width: 10 mm) as the working electrode and two Pt foils (widths: 10 and 20 mm) as the reference electrode and counter electrode, respectively, which are immersed into an IL-O or IL-T electrolyte. The Tafel plots are fitted in the electrochemical workstation. The cyclic voltammetry (CV) of Al plating/stripping and the overpotential curve are investigated with the Al-X/CC, CC, or Al foil (width: 10 mm) as the working electrode and two Al foils (widths: 5 and 15 mm) as the reference electrode and counter electrode. At the same time, all electrodes are immersed at 5 mm depth. For full batteries, the CVs of full batteries are tested at different scan rates over the range of 0.25–2.45 V. Also, electrochemical impedance spectra are recorded at a frequency range from 10^5 to 0.1 Hz. All the electrochemical measurements are carried on a BioLogic VMP-300 electrochemical workstation.

2.5 | Characterization techniques

The IL-O and IL-T electrolytes are inserted into a quartz capillary tube in the glovebox. Raman spectra are obtained $(200–700\,\mathrm{cm^{-1}})$ using a micro-Raman system (LABHRev-UV; Horiba). The morphologies are characterized by field emission scanning electron microscopy (FESEM; Zeiss Sigma). The surface of the carbon cloth is obtained from N_2 adsorption/desorption curves by a surface characterization analyzer (3Flex; Micromeritics). X-ray diffraction (XRD; Rigaku SmartLab) with Cu Kα radiation is used to determine the phase structure.

3 | RESULTS AND DISCUSSION

3.1 | Properties of the treated $AlCl_3$/[Emim]Cl IL electrolyte

An IL electrolyte with optimal Lewis acidity and high reactivity is necessary to achieve the cycle stability and anticorrosion of the anode.[5,25] For the preparation of the optimized IL electrolyte, we mix the anhydrous $AlCl_3$ and [EMIm]Cl at a molar ratio of 1.3:1 to obtain an original IL electrolyte (referred to as the "IL-O" electrolyte), followed by treatment with a high-purity Al pellet to obtain a colorless electrolyte (referred to as the "IL-T" electrolyte) (Figure 1A). The surface of the Al pellet is etched after treatment in an IL-O electrolyte (Figure S1). This condition is attributed to the reaction of Al with trace amounts of H_2O and HCl that probably arise from slight moisture contamination from the glovebox or the
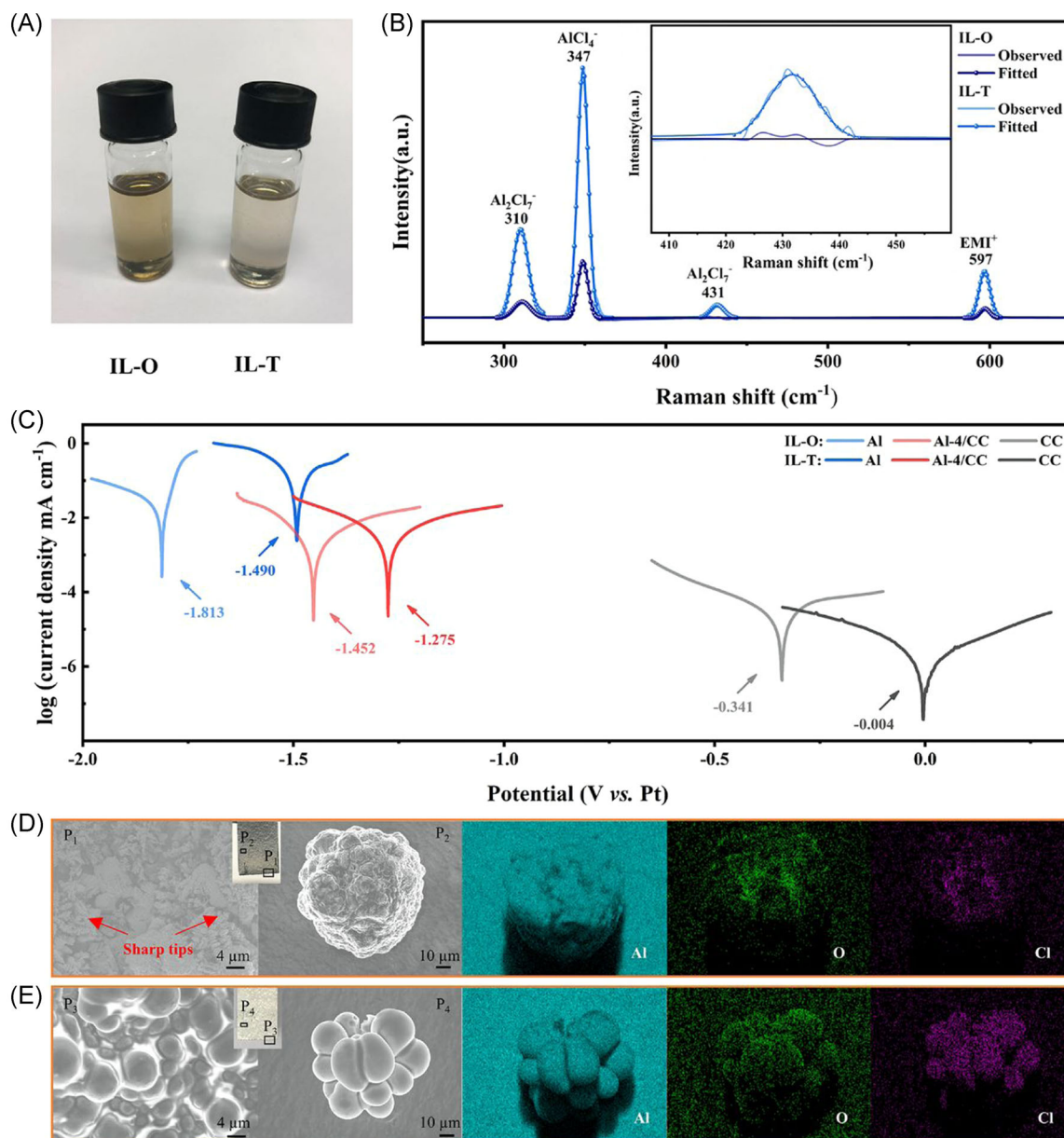
FIGURE 1 (A) Optical images and (B) Raman spectra of IL-O and IL-T electrolytes. (C) Potentiodynamic polarization curves using a three-electrode configuration (metallic Al foil, CC, and Al-4/CC as working electrodes, and Pt plate as counter and reference electrodes with IL-O and IL-T electrolytes) showing the corrosion of different electrodes. The SEM and elemental mapping images of 1 mAh cm^{-2} Al deposits with an Al foil as a substrate in (D) IL-O and (e) IL-T electrolytes. CC, current collector; IL-O, original ionic liquid; IL-T, treated ionic liquid; SEM, scanning electron microscopy

chemicals (HCl and $AlOCl_2^-$ or $AlOHCl_2$ are produced through the reaction of H_2O and $AlCl_3$).[26] The evolution of $AlCl_4^-$ and $Al_2Cl_7^-$ is investigated by Raman spectra in different stages (Figure 1B). After the treatment of the IL-O electrolyte, all the peaks become considerably stronger, and an $Al_2Cl_7^-$ peak appears at 431 cm^{-1}. This occurs due to the reaction of Al with HCl to again generate $AlCl_3$ via the following reaction:

$$Al + 3HCl \rightarrow AlCl_3 + 1/2H_2(g). \tag{1}$$
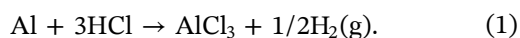
In addition, $AlCl_3$ further combines with Cl^- to produce $AlCl_4^-$, and then a portion of $Al_2Cl_7^-$ can be formed from further acid-based reactions via the following reactions:

$$AlCl_3 + Cl^- \rightarrow AlCl_4^-, \tag{2}$$

$$AlCl_3 + AlCl_4^- \rightarrow Al_2Cl_7^-. \tag{3}$$
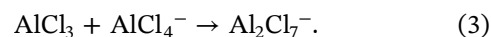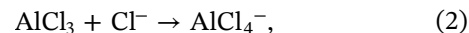
The corrosion of the Al metal foil is analyzed by a potentiodynamic polarization test in IL-O and IL-T

electrolytes (Figure 1C, blue colors, and Table S1). Compared with the IL-O electrolyte, the corrosion potential of the Al foil increases from −1.813 to −1.490 V, and the corrosion current reduces from 0.257 to 0.162 mA. This finding indicates that the IL-T electrolyte has a lower tendency to form a corrosion reaction to yield H_2 and a lower corrosion rate.[27,28] Thus, the strong corrosivity of chloroaluminate-based IL is ameliorated, and the metallic Al anode becomes stable in the presence of the IL-T electrolyte.

The Al foil electrodes with 1 mAh cm^{-2} loading are examined through scanning electron microscopy (SEM) and optical observations to gain insight into the different influences of the IL-O and IL-T electrolytes on Al plating. In Figure 1D, the edge position (P$_1$) of the Al foil in the IL-O electrolyte is overgrown with numerous sharp compounds, and the surface position (P$_2$) forms macroscopic aggregates with a rough surface caused by the irregular bulk stack. In contrast, with the IL-T electrolyte, the Al deposits on the edge (P$_3$) and surface (P$_4$) display a spherical stack with a smooth surface (Figure 1E). The chemical composition of Al deposits is analyzed through elemental mapping and X-ray spectroscopy. This process reveals the presence of Al, O, and Cl elements, and the Al elements in the IL-O electrolyte and IL-T electrolyte are 95.32 at% and 97.93 at%, respectively (Figures 1D,E, and S2). The high proportion of Al indicates a high quality of the deposited Al. However, the Al deposits show overgrowth preferentially at the edges due to the concentrated electric field and the convection of electrolyte flow. The Al deposits also show a non-adherent agglomerate at the 2D surface because the Al_2O_3-passivated surface film hinders the Al ion transfer at the electrode–electrolyte interphase (Figure S3).[14,26]

The behavior of Al deposition is monitored via in situ optical microscopy to visually track the dynamic morphology evolution of Al deposits on an Al foil. The Al deposits in the presence of the IL-O electrolyte are heterogeneous with black spots after plating for 3 min at the cross-section (Figure S4). After 30 min of electrodeposition, a crowd of visible bulges appear and continue to grow into dendritic and mossy Al. By contrast, in the presence of the IL-T electrolyte, a number of small crystal grains form at the cross-section after 3 min of electrodeposition. The Al deposits stack up into fluffy dendritic Al on the surface of the Al foil after 120 min of electrodeposition (Figure S5). The results indicate that the Al deposits in the IL-T electrolyte can sustainably eliminate the problem of dendrite formation. However, the features of all depositions on Al foil substrates, such as protuberant dendritic Al and

incompact connection with the substrate, demonstrate the unsolved dendrite formation issue in the Al metal anode, causing the short circuits and reducing the CE in aluminum–metal batteries.[14,29]

3.2 | Structural characterization of a 3D Al anode

As mentioned previously, the Al anode with IL-O electrolyte faces severe dendrite problems and corrosion during the electrochemical process. Although the IL-T electrolyte helps to decrease the corrosion and increase the quality of deposition, the Al anode still suffers from the problem of dendrite formation due to the inherent characteristics of the 2D metal foil with low active nucleation sites and low mobility of surface atoms (Figure 2A).[30,31] Here, the 3D Al anodes are used in Al electrodeposition with different capacities on the 3D carbon fiber of the carbon cloth (referred to as "Al-X/CC" electrodes, X = 2, 4, 6 mAh cm^{-2}). This condition suppresses Al dendrite formation by reducing the local current density with high effective surface areas per footprint area (Figure S6) and enhances the reversibility of Al metal during the electrochemical cycling by accommodating the volume change in the IL-T electrolyte (Figure 2A).

The corrosion of the Al-4/CC anode is shown in Figure 1C. It is clear that the Al-4/CC anode has a higher corrosion potential of −1.275 V and a lower corrosion current of 0.385 mA in the IL-T electrolyte compared with that of −1.452 V and 0.493 mA in the IL-O electrolyte. This finding is in good agreement with the results of Al anodes showing that the IL-T electrolyte has superior characteristics. From Table S1, it is clear that the 3D Al-4/CC anode always has a higher corrosion potential than the 2D Al foil anode in both IL-O and IL-T electrolytes. This situation is benefited from the anticorrosion effect of the carbon cloth in the IL electrolyte. The corrosion current of the planar Al foil anode is lower due to the protection of the passivating oxide layer.[19] The integration of fresh Al deposits with an anticorrosion CC substrate provides effective surface areas and conductive networks to increase the ionic and electronic conductivities and improve the activity of the electrochemical process. The 3D Al-4/CC anode is characterized by SEM to investigate the morphology of the Al deposits on carbon cloth. As shown on the top, in the presence of the IL-O electrolyte, the Al deposits form two structures: a grain stack and agglomerate with ~2 μm size (P5) and a sharp convex dendrite with a smaller grain (P6) on the carbon fiber surface (Figure 2B). By contrast, in the presence of the IL-T electrolyte, the Al deposits show a smooth, compact
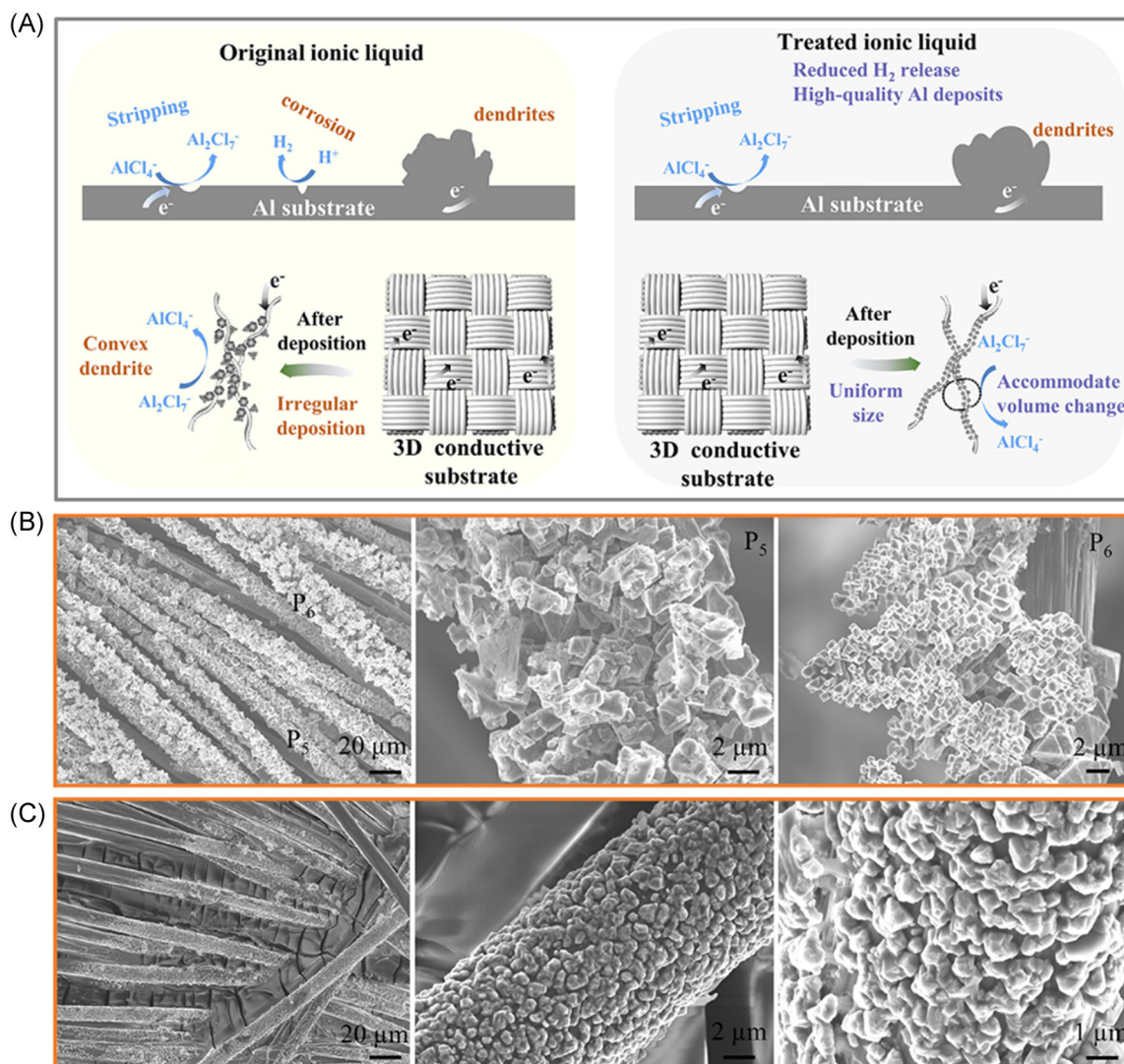
FIGURE 2 (A) Schematic illustration of the Al foil and the Al-*X*/CC anode in IL-O and IL-T electrolytes. SEM images of CC with a capacity of 4 mAh cm^{-2} after Al deposition in (B) IL-O and (C) IL-T electrolytes. CC, current collector; IL-O, original ionic liquid; IL-T, treated ionic liquid; SEM, scanning electron microscopy

and uniform coating on the carbon fiber surface with an ~1 µm grain size (Figure 2C). With the increase in the deposition capacity, the Al deposits expand along the carbon fiber surface and form a stable bond with the substrate (Figure S7).[32,33] Hence, in the presence of the IL-T electrolyte, the integrated 3D Al anode with superior Al deposits and uniform morphology can show better performance in aluminum–metal batteries than a 2D planar Al foil.

3.3 | Symmetric cell performance with a 3D Al anode

The electrochemical performance of the Al foil and Al-4/CC anodes is investigated in a symmetrical cell at

0.5 mA cm^{-2} using IL-O and IL-T electrolytes to evaluate the feasibility of the 3D Al anode (Figure 3A). The Al-4/CC symmetrical cell with the IL-T electrolyte shows a stable voltage profile with a lower voltage hysteresis of ~170 mV for 450 h and shows relatively flat voltage plateaus compared with Al foil anodes at the 5th, 50th, and 100th cycles (Figure 3A, inset). In comparison, in the Al symmetric cell with the IL-O electrolyte, a sudden drop in the voltage occurs after 84 h, recovers to normal at the 24th and 28th cycles, and subsequently drops again. This condition corresponds to the dendrite-induced short circuit of the cell. In the Al symmetric cell with the IL-T electrolyte, the voltage profile displays a massive fluctuation for 350 h until a complete loss of voltage occurs due to the destructive plating and stripping of Al.[34] At the different deposition capacities of 2 and 6 mAh cm^{-2},
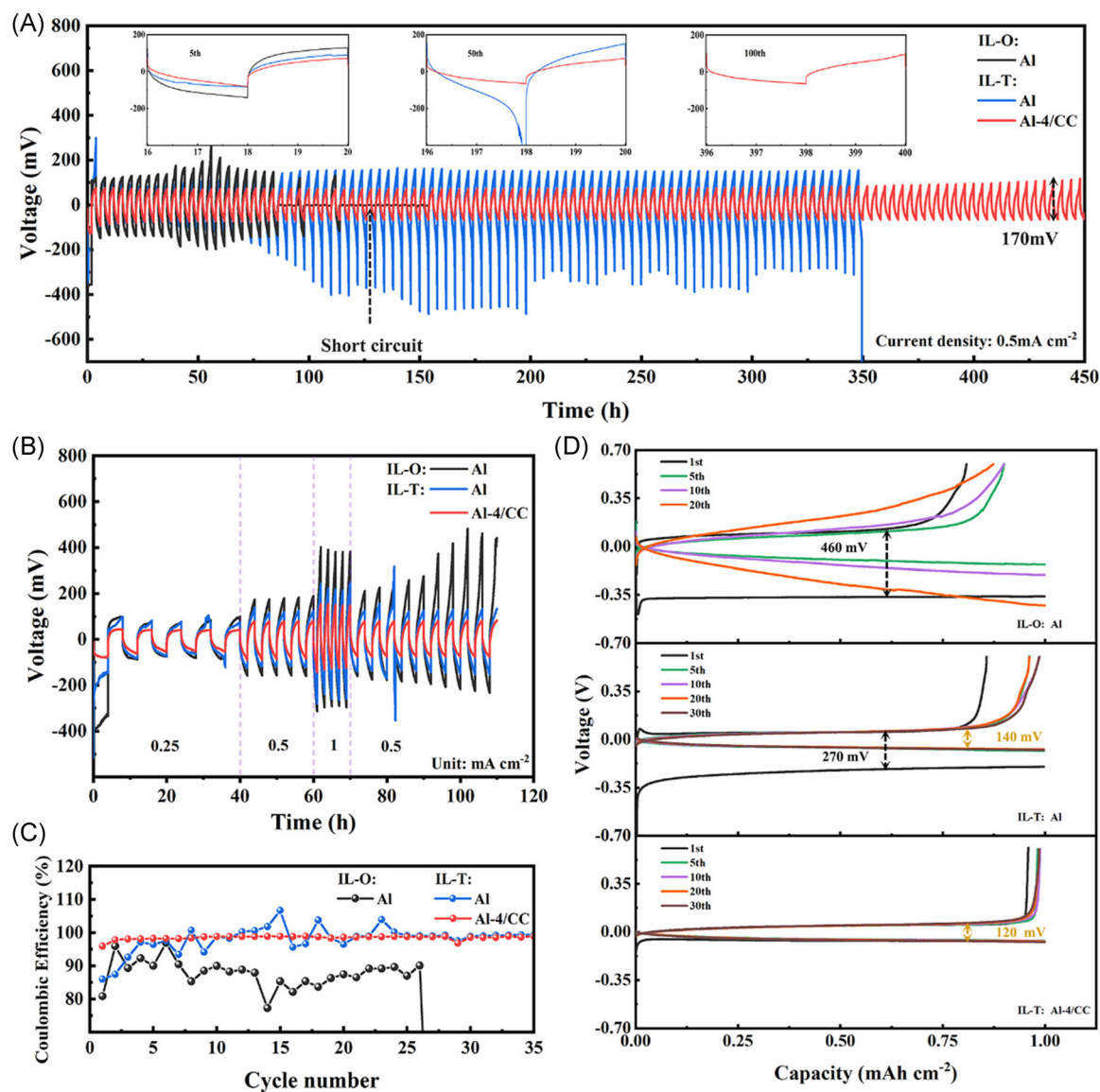
FIGURE 3 Al and Al-4/CC anodes with IL-O and IL-T electrolytes. (A) Voltage profiles of symmetrical cells at 0.5 mA cm^{-2}. (B) Rate performance of the symmetrical cells at current densities from 0.25 to 1 mA cm^{-2}. (C) CEs and (D) voltage profiles of the Al plating/stripping at 0.5 mA cm^{-2} with the capacity limited to 1 mAh cm^{-2}. CC, current collector; CE, Coulombic efficiency; IL-O, original ionic liquid; IL-T, treated ionic liquid

the electrochemical performance is inferior to that of the Al-4/CC anode due to the larger voltage hysteresis (Figure S8). The rate performance of different anodes is compared at a series of current densities, where the Al-4/CC anode shows lower voltage hysteresis compared with the Al anode using IL-O and IL-T electrolytes. When the current density increases from 0.25 to 1 mA cm^{-2}, the voltage hysteresis shows a steady growth of 100, 157, and 280 mV and remains unchanged when the current density is switched to 0.5 mA cm^{-2}. This finding suggests the low polarization and high stability of the Al-4/CC anode (Figures 3B and S9).

The Mo||Al and Mo||Al-4/CC cells are further assembled to elucidate the cycling reversibility of Al plating/stripping. The CE of Al plating/stripping can be calculated from the ratio of Al removed from the Mo substrate to that deposited during the same cycle. As shown in Figure 3C, the CE of Al anode with the IL-O electrolyte shows a strong fluctuation in the first eight cycles and is <90% until battery failure occurs after 26 cycles. The CE of the Al anode with the IL-T electrolyte starts to increase during the first five cycles and then fluctuates, exceeding 100%, which might be due to the residual Al in the former cycles. The CE remains stable at

~99.7% after 25 cycles. The CE of the Al-4/CC anode with the IL-T electrolyte is 95% at the beginning and then increases to ~99.7% after more than 35 cycles without attenuation. The high and stable CE reveals the enhanced reversibility of Al plating/stripping with the Al-4/CC anode. The charge–discharge voltage profiles are presented with different cycles at 0.5 mA cm^{-2} (Figure 3D). The Al anode with the IL-O electrolyte has higher voltage hysteresis at around 460 mV at the first cycle than that of the Al anode with the IL-T electrolyte at around 270 mV and lacks a stable discharge voltage plateau. However, the voltage hysteresis of the Al-4/CC anode with the IL-T electrolyte is only around 120 mV at the first cycle and maintains the same value without a polarization effect, which is lower than that of the Al anode with the IL-T electrolyte at 140 mV. The results comprehensively demonstrate the validity of the IL-T electrolyte and the 3D Al-4/CC anode for reversibility and stability during Al plating/stripping.

The Al nucleation overpotentials (the magnitude of the voltage spike at the onset of Al deposition) are significant parameters to identify the Al plating process for understanding the course of dendrite formation.[35−37] Figure 4A shows the characteristic voltage profiles during Al deposition on different anodes. The Al foil anodes using IL-O and IL-T electrolytes show a voltage dip at the beginning of Al deposition. The nucleation overpotential using the IL-T electrolyte is as high as 1133 mV, which is higher than that using the IL-O electrolyte (783 mV). This condition is due to the difficult consumption of Al$_2$O$_3$ oxide layer on the Al surface in IL-T electrolyte. By contrast, the nucleation overpotential of CC is 178 mV, which is smaller than those of 2D Al anodes. The lower resistance of Al nucleation can be attributed to the increased surface area, which reduces the local current density and yields more nucleation sites, thereby suppressing Al dendrite formation.[37,38] The Al-4/CC anode with 4 mAh cm^{-2} predeposits tends to induce postnucleation growth without a sharp voltage spike, providing stable and favorable conditions for the deposition of Al$_2$Cl$_7$$^-$. Similarly, the Al-2/CC anode has a small nucleation overpotential due to the few Al deposits on the CC surface. In this case, the Al-6/CC anode shows a quick response for nucleation growth with a less bare surface of CC, which is in accordance with Al and Al-4/CC anodes (Figure S10). The reduced nucleation barrier is crucial for facilitating smooth deposition and achieving high-rate performance.

Figure 4B shows the CV curves of symmetrical cells with different anodes in the second cycle. The curves of the Al anode using IL-O and IL-T electrolytes form a loop during the plating of bulk Al electrodeposition (the reduction reaction); this condition is attributed to the high overpotential necessary to form the first nuclei and the growth of metallic aluminum on the Al anode.[39,40] During the stripping process, the oxidation peak (Category B) current is 9 mA, which is the same as the reduction peak (Category C), suggesting the reversible Al stripping/plating process with the Al anode using IL-O and IL-T electrolytes. The CC results in a relatively high-peak current due to the porous structure for Al stripping/plating on the carbonaceous surface. The curve of the Al-4/CC anode has an additional oxidation peak (Category A) that arises from the stripping of Al from the bulk Al on the CC surface.[32] The sharp redox peak and the high current density of the Al-4/CC anode indicate better ion diffusion kinetics and superior Al plating/stripping reversibility.

Figures 4C and 4D show the changes in the morphologies of the Al foil and Al-4/CC anodes from the combination of SEM and optical images after 10 cycles in the presence of the IL-T electrolyte. The Al foil anode is consumed and pulverized with enormous pits and cracks (the red dotted lines in Figure 4C) due to uncontrolled plating/stripping. The consumption and pulverization gradually destroy the metallic Al anode, leading to capacity degradation and breakage of the battery. By contrast, the Al-4/CC anode retains the original structure from the optical image (Figure 4D). The grain sizes of the uniformly distributed Al deposits change and cover large areas of the surface of the carbon fiber. Some Al deposits aggregate into microscale Al crystals and form a conformal Al coating layer in some areas (Figure 4D). These results confirm that the 3D Al-4/CC anode can accommodate the volume change in Al deposits during plating/stripping due to the large space between the carbon fibers and strong bonding between Al deposits and the CC substrate.[41] The phase evolution of the Al-4/CC anode is verified on the basis of the XRD data where only metallic Al peaks can be observed without any purities, except for the carbon peak in the CC substrate (Figure 4E). After several cycles, the XRD pattern show some peaks belonging to Al oxide or other components due to repeated plating/stripping. However, these peaks mainly originated from the metallic Al peaks. These results confirm that the 2D Al anode is highly irreversible with continuous consumption and dendrite growth during cycling. However, the Al-4/CC anode with a conductive substrate can effectively enhance Al plating and stripping, thereby improving cycling stability and reversibility (Figure 4F).

3.4 | High-performance full battery

Graphite is used as the cathode to couple with Al and Al-4/CC anodes in presence of the IL-T electrolyte to
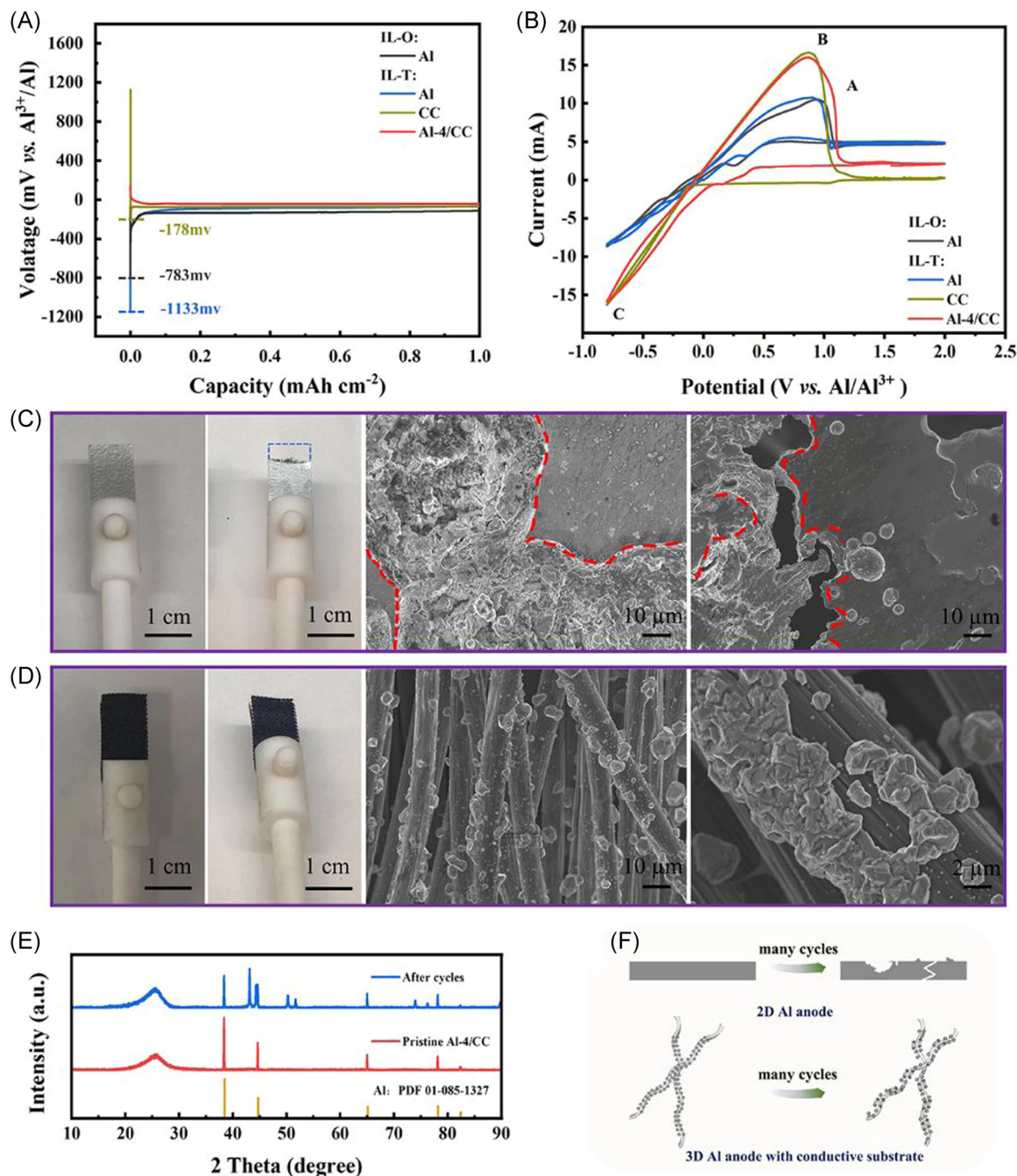
FIGURE 4 (A) Voltage curves during Al nucleation at $0.5\,mA\,cm^{-2}$ on Al, bare CC, and Al-4/CC electrodes. (B) CV curves of Al plating/stripping at $1\,mV\,s^{-1}$. Surface morphology of (C) the Al foil anode and (D) the Al-4/CC anode in the presence of the IL-T electrolyte after 10 cycles at $0.5\,mA\,cm^{-2}$. (E) XRD pattern of the Al-4/CC anode before and after 10 cycles in the presence of the IL-T electrolyte. (F) Schematic illustration of the cycling of the 2D Al foil and the 3D Al-X/CC anode in the presence of IL-T electrolytes. CC, current collector; CV, cyclic voltammetry; IL-T, treated ionic liquid; XRD, X-ray diffraction

fabricate aluminum–graphite batteries (Figure 5A). This process is performed to demonstrate the effectiveness and practicability of our strategy in a full battery. The full battery with the Al-4/CC anode has high cycling stability with an initial discharge capacity of $94\,mAh\,g^{-1}$ and retains a discharge capacity of $76\,mAh\,g^{-1}$ after 200 cycles, corresponding to a capacity retention of 80%. By contrast,

the battery with the Al anode shows a 60% capacity retention with $92\,mAh\,g^{-1}$ initial discharge capacity and $60\,mAh\,g^{-1}$ initial discharge capacity after 200 cycles, confirming the superior durability and high-capacity performance of the Al-4/CC anode. The CE of the Al-4/CC anode is slightly lower in the full battery than that of the Al anode; this is ascribed to adverse side
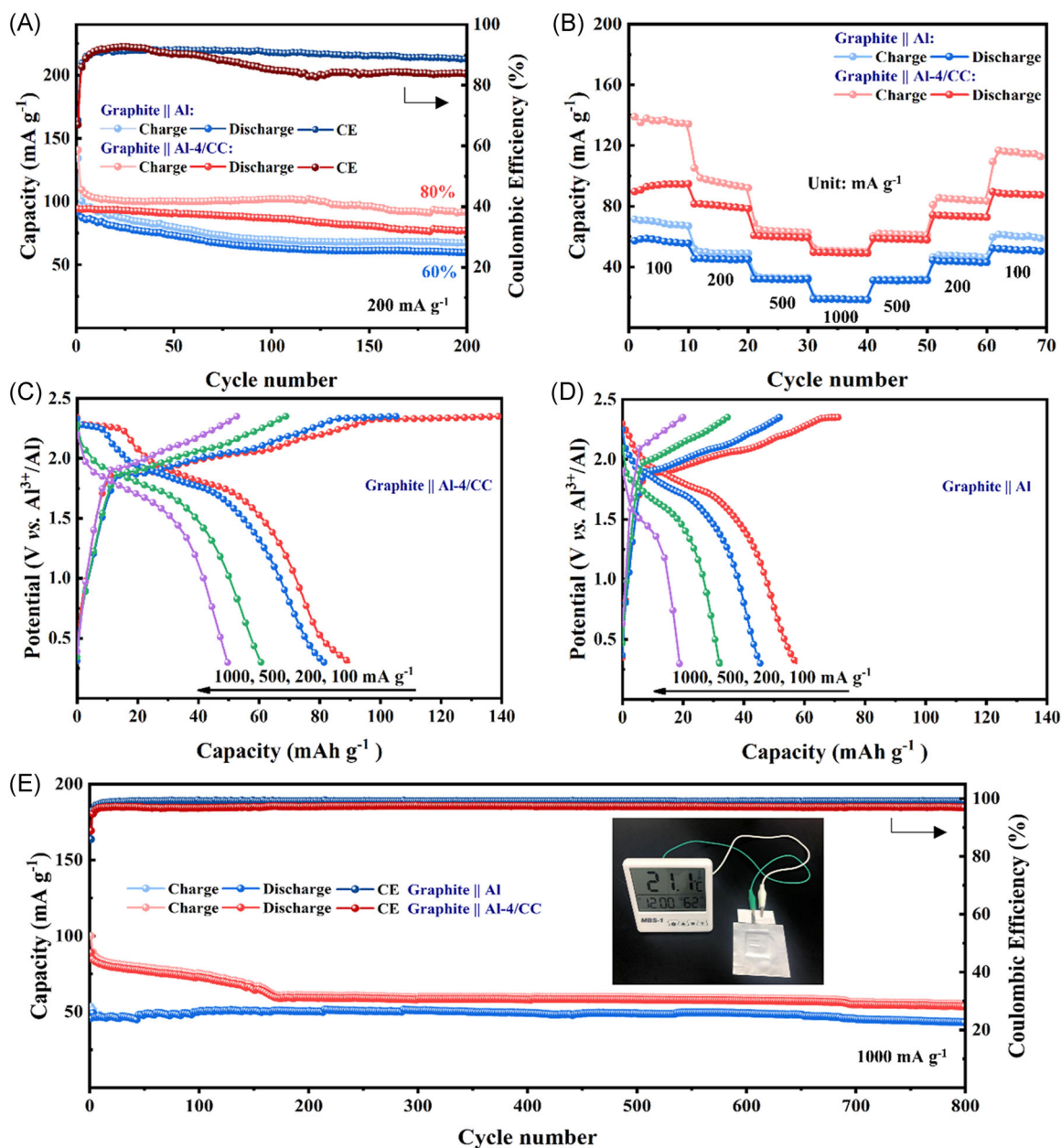
FIGURE 5 Electrochemical performance of the graphite∥Al and graphite∥Al-4/CC batteries in the IL-T electrolyte: (A) cycling performance at 200 mA g^{-1}. (B) Rate performance at different current densities. Corresponding voltage profiles at different rates with (C) Al-4/CC and (D) Al anodes. (E) Long cycling performance at 1000 mA g^{-1}. CC, current collector; IL-T, treated ionic liquid

reactions due to the higher surface area of the anode.[42] For the rate capacity test, the reversible capacity using the Al-4/CC anode maintains 50 mAh g^{-1} discharge capacity at a high current density of 1000 mA g^{-1} and retains 88 mAh g^{-1} discharge capacity when the current density returns to 100 mA g^{-1} (Figure 5B). The obvious inferior result with the Al anode is clear from the discharge capacities of 18 and 52 mAh g^{-1} obtained for a current density in the range of 1000–100 mA g^{-1}. The corresponding charge–discharge profiles at different current densities are shown in Figure 5C,D. The battery

with the Al-4/CC anode shows a clear discharge voltage plateau in the range of 1.5–2.0 V and smaller polarization than that with the Al anode. This indicates that the Al plating/stripping process is promoted by the use of the 3D structure anode, which is in agreement with the increased redox peak in the CV measurement (Figure 4B). This excellent rate performance of the graphite∥Al-4/ CC battery is ascribed to the small charge-transfer resistance and superior kinetics due to the high specific surface area and good electric conductivity. Electrochemical impedance spectroscopy is performed for the

full batteries (Figure S11). The charge-transfer resistance of the full battery with the Al-4/CC anode is smaller than that with the Al anode, indicating the fast charge-transfer kinetics due to the 3D conductive network and the high reaction area. The full battery shows long-term cycling stability with Al and Al-4/CC anodes (Figure 5E). The graphite‖Al-4/CC battery delivers a high initial discharge capacity of 89 mAh g^{-1} and stabilizes at 54 mAh g^{-1} after 800 cycles, with a high CE of 97% at 1000 mA g^{-1}. Also, the battery can easily power a digital thermometer and hygrometer (Figure 5E, inset). After

cycling, the discharge capacity of the graphite‖Al battery drops to 43 mAh g^{-1} with a high CE of 99% from the low initial discharge capacity of 50 mAh g^{-1}. These results reveal the infinite potential of the Al-4/CC anode for full battery applications.

CV measurements are performed to evaluate the battery storage behavior and kinetics at various scan rates from 0.4 to 1.0 mV s^{-1}. This process is conducted to analyze the excellent rate performance of the full battery. As shown in Figure 6A,B, the reduction peaks shift to a lower potential with the increase in the scan rate,
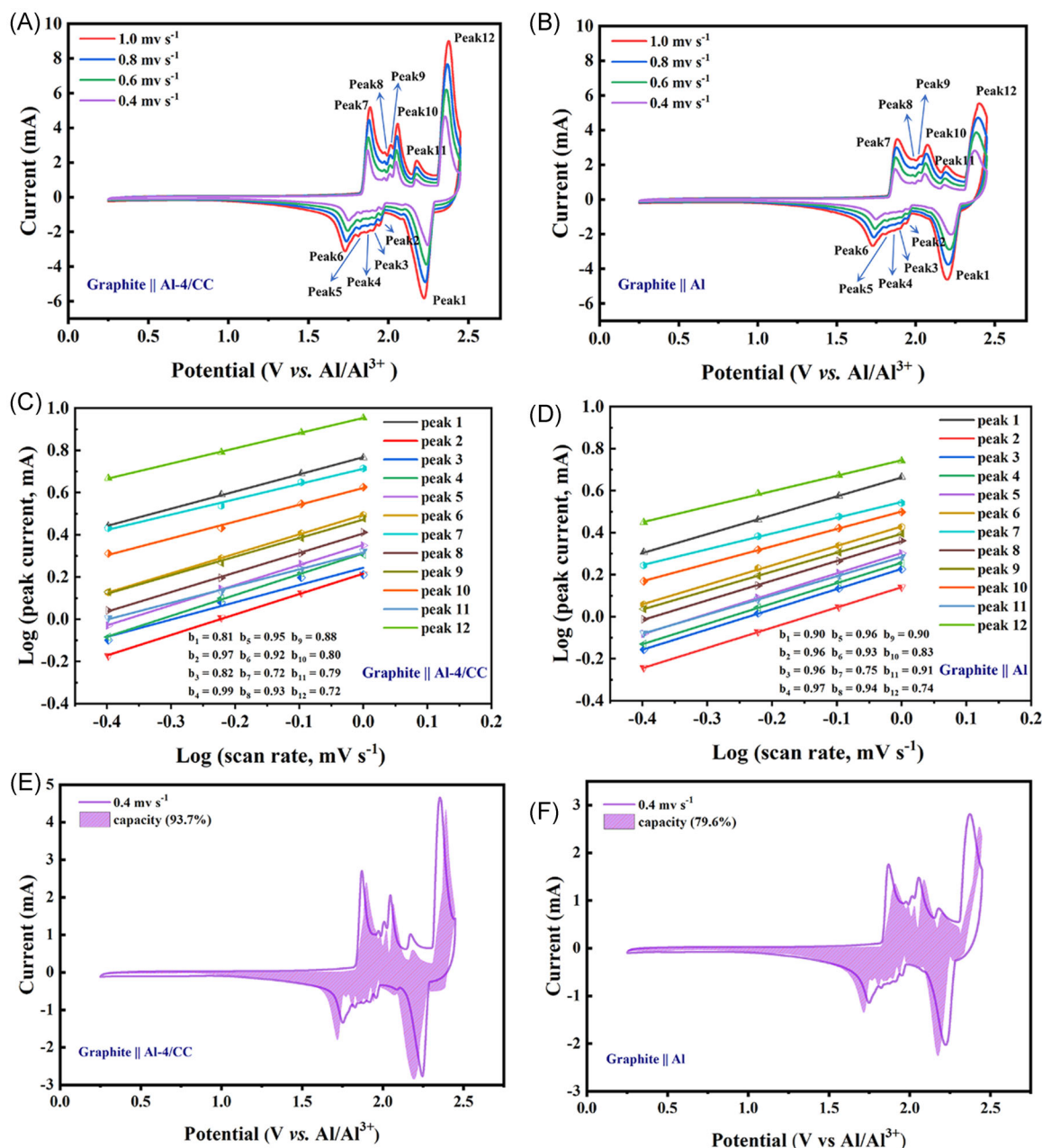
FIGURE 6 CV curves at different scan rates from 0.4 to 1 mV s^{-1} with (A) Al-4/CC and (B) Al foil anodes. Corresponding log (peak current) versus log (scan rate) plots for each redox peak with (C) Al-4/CC and (D) Al foil anodes. Capacitive contribution at 0.4 mV s^{-1} with (E) Al-4/CC and (F) Al foil anodes. CC, current collector; CV, cyclic voltammetry; IL-T, treated ionic liquid; XRD, X-ray diffraction

whereas the oxidation peaks shift to a higher potential due to capacitive-controlled behavior.

The relationship between peak currents (i) and scan rates (v) can reflect the capacity contribution by diffusion and capacitive behavior as follows:

$$i = av^b, \tag{4}$$

$$\log(i) = b \log(v) + \log(a), \tag{5}$$

where a and b are adjustable constants. The diffusion-controlled process dominates the electrochemical reaction when the b value is approximately 0.5. When the b value is close to 1, the electrochemical reaction is a capacitive-controlled process. The corresponding b values of 12 peaks are 0.81, 0.97, 0.82, 0.99, 0.95, 0.92, 0.72, 0.93, 0.88, 0.80, 0.79, and 0.72, respectively, for the Al-4/CC anode. This finding indicates that the capacity distribution of the capacitive-controlled process plays a major role in the performance of the full battery (Figure 6C).[43] Combined with those values from Al anode (Figure 6D), a considerable capacitive-controlled portion takes part in the aluminum–graphite battery causing the fast ion diffusion kinetics. As shown in Figure 6E, the capacitive-controlled contribution reaches up to 93.7% of the total capacity at $0.4\,\mathrm{mV\,s^{-1}}$ with the Al-4/CC anode, which is higher than that with the Al anode (79.6%, Figure 6F). The capacity contribution increases with the increase in the scan rate from 93.7% to 98.7% using the Al-4/CC anode and from 79.6% to 86.7% using the Al anode (Figure S12). The superior rate performance of the graphite||Al-4/CC battery is due to the high ratio of the capacitive-controlled behavior and fast ion transfer kinetics.

4 | CONCLUSION

In this study, we demonstrate a novel electrodeposition strategy to prepare an optimized 3D Al anode, such as Al-4/CC. The prepared anode suppresses Al dendrite formation, accommodates volume change, and provides a fast kinetic electron reaction with the IL-T electrolyte. The CC substrate for the 3D Al anode provides a high specific surface area and conductivity to lower the local current density and nucleation overpotential. The Al-4/CC anode delivers a 450 h lifespan and high reversibility of 99.7% CE during Al plating/stripping. The full battery with a graphite cathode shows a much-improved capacity of $54\,\mathrm{mAh\,g^{-1}}$ at $1000\,\mathrm{mA\,g^{-1}}$ after 800 cycles compared with the planar Al anode under the same tested conditions. This study highlights the importance of a rational design principle of a 3D Al anode for the practical application of aluminum–metal batteries.

CONFLICT OF INTERESTS
The authors declare no conflict of interests.

ORCID
Kwan San Hui http://orcid.org/0000-0001-7089-7587
Fuming Chen http://orcid.org/0000-0002-0108-9831
Zongping Shao http://orcid.org/0000-0002-4538-4218
Kwun Nam Hui http://orcid.org/0000-0002-3008-8571

REFERENCES
1. Yang H, Li H, Li J, et al. The rechargeable aluminum battery: opportunities and challenges. *Angew Chem Int Ed*. 2019;58(35):11978-11996.
2. Zhang Y, Liu S, Ji Y, Ma J, Yu H. Emerging nonaqueous aluminum-ion batteries: challenges, status, and perspectives. *Adv Mater*. 2018;30(38):1706310.
3. Elia GA, Marquardt K, Hoeppner K, et al. An overview and future perspectives of aluminum batteries. *Adv Mater*. 2016;28(35):7564-7579.
4. Wang S, Jiao S, Wang J, et al. High-performance aluminum-ion battery with CuS@C microsphere composite cathode. *ACS Nano*. 2016;11(1):469-477.
5. Wu F, Yang H, Bai Y, Wu C. Paving the path toward reliable cathode materials for aluminum-ion batteries. *Adv Mater*. 2019;31(16):1806510.
6. Wang S, Yu Z, Tu J, et al. A novel aluminum-ion battery: Al/AlCl₃-[EMIm]Cl/Ni₃S₂@graphene. *Adv Energy Mater*. 2016;6(13):1600137.
7. Kravchyk KV, Kovalenko MV. Aluminum electrolytes for Al dual-ion batteries. *Commun Chem*. 2020;3(1):120.
8. Sun H, Wang W, Yu Z, Yuan Y, Wang S, Jiao S. A new aluminium-ion battery with high voltage, high safety and low cost. *Chem Comm*. 2015;51(59):11892-11895.
9. Lin M-C, Gong M, Lu B, et al. An ultrafast rechargeable aluminium-ion battery. *Nature*. 2015;520(7547):324-328.
10. Xu H, Chen H, Lai H, et al. Capacitive charge storage enables an ultrahigh cathode capacity in aluminum-graphene battery. *J Energy Chem*. 2020;45:40-44.
11. Huang H, Zhou F, Lu P, et al. Design and construction of few-layer graphene cathode for ultrafast and high-capacity aluminum-ion batteries. *Energy Stor Mater*. 2020;27:396-404.
12. Zhou Z, Li N, Wang P, et al. All-carbon positive electrodes for stable aluminium batteries. *J Energy Chem*. 2019;42:17-26.

13. Li M, Lu J, Ji X, et al. Design strategies for nonaqueous multivalent-ion and monovalent-ion battery anodes. *Nat Rev Mater.* 2020;5(4):276-294.

14. Long Y, Li H, Ye M, et al. Suppressing Al dendrite growth towards a long-life Al-metal battery. *Energy Stor Mater.* 2021; 34:194-202.

15. Leisegang T, Meutzner F, Zschornak M, et al. The aluminum-ion battery: a sustainable and seminal concept? *Front Chem.* 2019;7:268.

16. Wang S, Jiao S, Tian D, et al. A novel ultrafast rechargeable multi-ions battery. *Adv Mater.* 2017;29(16):1606349.

17. Jiao H, Jiao S, Song W-L, et al. Al homogeneous deposition induced by N-containing functional groups for enhanced cycling stability of Al-ion battery negative electrode. *Nano Res.* 2021;14(3):646-653.

18. Liang Y, Dong H, Aurbach D, Yao Y. Current status and future directions of multivalent metal-ion batteries. *Nat Energy.* 2020; 5(9):646-656.

19. Chen H, Xu H, Zheng B, et al. Oxide film efficiently suppresses dendrite growth in aluminum-ion battery. *ACS Appl Mater Interfaces.* 2017;9(27):22628-22634.

20. Choi S, Go H, Lee G, Tak Y. Electrochemical properties of an aluminum anode in an ionic liquid electrolyte for rechargeable aluminum-ion batteries. *Phys Chem Chem Phys.* 2017; 19(13):8653-8656.

21. Yan C, Lv C, Wang L, et al. Architecting a stable high-energy aqueous Al-ion battery. *J Am Chem Soc.* 2020;142(36): 15295-15304.

22. Jiao H, Jiao S, Song WL, et al. Cu-Al composite as the negative electrode for long-life Al-ion batteries. *J Electrochem Soc.* 2019; 166(15):A3539.

23. Wang J, Jiao H, Song W-L, et al. Stable interface between a NaCl-AlCl$_3$ melt and a liquid Ga negative electrode for a long-life stationary Al-ion energy storage battery. *ACS Appl Mater Interfaces.* 2020;12(13):15063-15070.

24. Shen X, Sun T, Yang L, et al. Ultra-fast charging in aluminum-ion batteries: electric double layers on active anode. *Nat Commun.* 2021;12:820.

25. Chen X, Yao X, Wang C, Chen L, Chen X. Anion-effects on electrochemical properties of ionic liquid electrolytes for rechargeable aluminum batteries. *J Mater Chem A.* 2015;3(45): 22677-22686.

26. Vaughan J, Dreisinger D. Electrodeposition of aluminum from aluminum chloride-trihexyl(tetradecyl) phosphonium chloride. *J Electrochem Soc.* 2008;155(1):D68.

27. Zhao Z, Zhao J, Hu Z, et al. Long-life and deeply rechargeable aqueous Zn anodes enabled by a multifunctional brightener-inspired interphase. *Energy Environ Sci.* 2019;12:1938-1949.

28. Ma L, Chen S, Li N, et al. Hydrogen-free and dendrite-free all-solid-state Zn-ion batteries. *Adv Mater.* 2020;32(14): 1908121.

29. Dai H, Xi K, Liu X, Lai C, Zhang S. Cationic surfactant-based electrolyte additives for uniform lithium deposition via lithiophobic repulsion mechanisms. *J Am Chem Soc.* 2018; 140(50):17515-17521.

30. Lu Y, Tu Z, Archer LA. Stable lithium electrodeposition in liquid and nanoporous solid electrolytes. *Nat Mater.* 2014;13(10):961-969.

31. Park S, Jin HJ, Yun YS. Advances in the design of 3D-structured electrode materials for lithium-metal anodes. *Adv Mater.* 2020;32(51):2002193.

32. Zhang M, Watson JS, Counce RM, Trulove PC, Zawodzinski TA. Electrochemistry and morphology studies of aluminum plating/stripping in a chloroaluminate ionic liquid on porous carbon materials. *J Electrochem Soc.* 2014;161(4): D163.

33. Tang J, Azumi K. Optimization of pulsed electrodeposition of aluminum from AlCl$_3$-1-ethyl-3-methylimidazolium chloride ionic liquid. *Electrochim Acta.* 2011;56(3): 1130-1137.

34. Long Y, Li H, Ye M, et al. Suppressing Al dendrite growth towards a long-life Al-metal battery. *Energy Stor Mater.* 2020; 34:194-202.

35. Pei A, Zheng G, Shi F, Li Y, Cui Y. Nanoscale nucleation and growth of electrodeposited lithium metal. *Nano Lett.* 2017; 17(2):1132-1139.

36. Biswal P, Stalin S, Kludze A, Choudhury S, Archer LA. Nucleation and early stage growth of Li electrodeposits. *Nano Lett.* 2019;19(11):8191-8200.

37. Zeng Y, Zhang X, Qin R, et al. Dendrite-free zinc deposition induced by multifunctional CNT frameworks for stable flexible Zn-ion batteries. *Adv Mater.* 2019;31(36):1903675.

38. Cohn AP, Muralidharan N, Carter R, Share K, Pint CL. Anode-free sodium battery through in situ plating of sodium metal. *Nano Lett.* 2017;17(2):1296-1301.

39. Muñoz-Torrero D, Leung P, García-Quismondo E, et al. Investigation of different anode materials for aluminium rechargeable batteries. *J Power Sources.* 2018;374:77-83.

40. Jiang T, Chollier Brym MJ, Dubé G, Lasia A, Brisard GM. Electrodeposition of aluminium from ionic liquids: part II-studies on the electrodeposition of aluminum from aluminum chloride (AlCl$_3$)-trimethylphenylammonium chloride (TMPAC) ionic liquids. *Surf Coat Technol.* 2006;201(1):10-18.

41. Jin S, Jiang Y, Ji H, Yu Y. Advanced 3D current collectors for lithium-based batteries. *Adv Mater.* 2018;30(48):1802014.

42. Lindahl N, Bitenc J, Dominko R, Johansson P. Aluminum metal-organic batteries with integrated 3D thin film anodes. *Adv Funct Mater.* 2020;30(51):2004573.

43. Wang X, Xi B, Ma X, et al. Boosting zinc-ion storage capability by effectively suppressing vanadium dissolution based on robust layered barium vanadate. *Nano Lett.* 2020;20(4): 2899-2906.

AUTHOR BIOGRAPHIES

Junfeng Li received his Masters degree in 2019 from the University of Science and Technology Beijing. He is currently pursuing a PhD under the supervision of Prof. Kwun Nan Hui at the Institute of Applied Physics and Materials Engineering, University of Macau. His research focuses on preparing advanced electrode

materials and the design of battery systems, including aluminum-ion batteries and potassium-ion batteries.

Kwan San Hui is a reader in Mechanical Engineering of School of Engineering, University of East Anglia. He obtained his PhD degree in Mechanical Engineering at the Hong Kong University of Science and Technology (2008). His research focuses on advanced materials for energy storage, conversion and electrocatalysis.

Shunping Ji was born in Yunnan province, China. He received his MS degree in Green Chemistry from the University of Sichuan in 2013. He is currently a doctoral candidate in the Institute of Applied Physics and Materials Engineering at the University of Macau, working on nanocomposites for energy storage under the supervision of Prof. Kwun Nam Hui.

Chenyang Zha is a researcher of the Macau Young Scholars Program at the Institute of Applied Physics and Materials Engineering of University of Macau. He received his PhD degree in Chemistry from Nanjing Tech University and Uppsala University in 2016, and then he moved to Soochow University and State University of New York to complete a postdoctoral training before taking the current position in 2019. His research focuses on novel functional materials for energy applications, particularly in the realm of advanced batteries and electrocatalysts.

Cheng-Zong Yuan received his PhD degree from the University of Science and Technology of China in 2019. He is currently a postdoctoral researcher at at the Institute of Applied Physics and Materials Engineering of University of Macau. His research interests focus on designing nanomaterials for energy storage and conversion, such as water splitting, metal-air batteries, and CO_2 electroreduction.

Shuxing Wu received his PhD degree in School of Materials Science and Engineering at the Pusan National University in South Korea in 2018. Then, he joined the Energy and Chemical Engineering Faculty at the Guangdong University of Technology in Guangzhou City. His current research interests focus on electrochemical energy storage, including lithium-ion batteries and lithium-sulfur batteries.

Feng Bin is an Associate Professor in State Key Laboratory of High Temperature Gas Dynamics, Institute of Mechanics, Chinese Academy of Sciences. He received his PhD degree in Tianjing University in 2011. His current research interests focus on catalytic combustion and pollutant control technology.

Xi Fan obtained his PhD degree in Condensed Matter Physics from Wuhan University in 2013. He was then a postdoctoral researcher at The Hong Kong Polytechnic University from 2015 to 2017, and in 2017 he was promoted to Associate Professor at Ningbo Institute of Materials Technology and Engineering, Chinese Academy of Sciences (CAS). His research interests focus on the development of flexible organic solar cells, perovskite solar cells, and quantum dot light-emitting diodes.

Fuming Chen is a Professor of School of Physics and Telecommunication Engineering, South China Normal University. He received his PhD degree from the Nanyang Technological University at Singapore in 2010. His current research interests are focused on advanced functional materials for energy storage, electrochemical desalination and photo/electrochemical catalysis.

Zongping Shao is a John Curtin Distinguished Professor at Curtin University, Australia, and also a Professor at Nanjing Tech University, China. He obtained his PhD degree from Dalian Institute of Chemical Physics, China, in 2000. He worked as a Visiting Scholar at Institut

de Researches Sur La Catalyse, CNRS, France, and then a Postdoctoral Fellow at California Institute of Technology, USA, from 2000 to 2005. His current research interests include fuel cells, lithium-ion batteries, metal-air batteries, solar cells, and oxygen-permeable membranes. He has been recognized as a Highly-Cited Researcher by Clarivate Analytics since 2017.

Kwun Nam Hui is an Associate Professor of the Institute of Applied Physics and Materials Engineering, University of Macau. He obtained his PhD degree from The University of Hong Kong (2009). His research focuses on electrochemical energy storage and conversion.

SUPPORTING INFORMATION

Additional Supporting Information may be found online in the supporting information tab for this article.